Crystal-structure, magnetic-susceptibility, and EPR studies of bis(piperidinium)tetrabromocuprate(II): A novel monomer system showing spin diffusion

Baldev R. Patyal,* Brian L. Scott, and Roger D. Willett
Chemical Physics Program, Washington State University, Pullman, Washington 99164-4620
(Received 10 July 1989)

The crystal structure of the compound, bis(piperidinium)tetrabromocuprate(II) [$(pipdH)_2CuBr_4$] is monoclinic, space group $P2_1/c$, with $a=8.487(2)$ Å, $b=17.225(3)$ Å, $c=12.380(2)$ Å, and $\beta=99.29(2)°$. The structure consists of isolated, flattened $CuBr_4^{2-}$ tetrahedra. Close Br $\cdots$ Br contacts (4.10 Å) occur between tetrahedra related by a center of inversion, defining magnetic dimeric units. Additional Br $\cdots$ Br contacts (4.30 Å) occur between dimeric units related by unit-cell translations in the a direction. This defines a double chain of dimers in which $CuBr_4^{2-}$ ions are all magnetically equivalent. The crystal symmetry generates a second type of crystallographically equivalent, but magnetically inequivalent, chain in the structure. Magnetic-susceptibility data indicate the presence of dominant antiferromagnetic coupling. The system is best characterized magnetically as exchange-coupled $CuBr_4^{2-}$ dimers ($J/k=-6.64$ K), with a weaker one-dimensional coupling ($J'/k=-0.66$ K) between these dimeric units. The room-temperature EPR data in the a-c^* and a-b planes indicate the presence of strong spin-diffusive relaxation processes defining the system as a linear chain propagating along the a axis. This is the first copper bromide compound to our knowledge which shows spin-diffusive behavior. In the b-c^* plane, the EPR spectra at various orientations are the superposition of the spectra corresponding to two magnetically inequivalent subsystems, with the magnitude of the interaction between the subsystems, J_i, determined to be equal to 0.002 K. Thus, structurally this compound is a monomer, magnetically it can be characterized as a dimer, and EPR studies show that dynamically it behaves as a linear chain propagating along the crystallographic a axis.

I. INTRODUCTION

As part of the general interest in low-dimensional magnetism[1] in the solid-stae community, the experimental study of magnetostructural correlations in copper(II) halides has been a fruitful area of research in this laboratory for several years. In these halocuprate(II) systems, the copper(II) ion is capable of assuming a variety of coordination geometries, involving fourfold-, fivefold-, and sixfold-coordinated species. Oligomeric and/or polymeric species are subsequently formed by sharing corners, edges, or faces of these coordination polyhedra. Thus, the magnetic exchange occurs via single halide Cu-X-Cu pathways where the magnetic orbitals on the two copper(II) ions overlap through one or more common bridging halide ions. Our emphasis has centered upon the effect that changes in the coordination geometry and the polyhedra linkage have upon the sign and strength of the magnetic coupling.[2] This has led to the synthesis and characterization of a number of interesting and significant systems. Included have been (a) the first good one-dimensional (1D) spin-$\frac{1}{2}$ ferromagnets[3] for which one analog, (cyclohexylammonium)tribromocuprate(II), has been used to clearly demonstrate the existence of magnetic solitons,[4] (b) the control of the magnitude and anisotropy of exchange interaction J, in the layer perovskite A_2CuX_4 series,[5] and (c) systems containing subunits with an odd number of Cu(II) ions, which may lead to interesting spin frustration[6] and ferrimagnetic behavior.[7]

Recently, it has been recognized that the exchange interaction between the magnetic subsystems (oligomers, chains, and layers) in these systems may become quite significant when there are close halide-halide contacts. This was demonstrated clearly in a series of studies by Drumheller and co-workers on layer perovskites of the form $(NH_3C_nH_{2n}NH_3)CuX_4$.[8] For large n they behave as quasi-2D ferromagnets; as n decreases, the interlayer contacts shorten and strong antiferromagnetic coupling between layers is turned on. In fact, for $n=2$, $X=$Br, the system is dominated by the interlayer coupling and is better characterized as a 1D antiferromagnet. Similar phenomena have been observed in other systems as well.[9] In general, it appears that significant exchange occurs ($J/k>1$ K) when the $X\cdots X$ contact distance between magnetic subsystem is within $2r+0.5$ Å, where r is the van der Waals radius of the halide ion.

In the study of exchange interaction between paramagnetic centers, magnetic-susceptibility measurements[10] and EPR measurements[11] have contributed significantly. Combined with x-ray diffraction studies, they lead to the data required for the delineation of magnetostructural correlations. The information provided by these measurements can be combined to give unequivocal answers which none of them can provide individually. In this paper, the results of these studies on the compound bis(piperidinium)tetrabromocuprate(II) [$(pipdH)_2CuBr_4$] are presented and utilized to derive a comprehensive picture of its magnetic behavior.

TABLE I. Crystallographic data for bis(piperidinium) tetrabromocuprate(II) $[(C_5H_{12}N_2)_2CuBr_4]$.

	Formula weight 553.46
$a=8.487(2)$ Å	Space group $P2_1/c$ (no. 14)
$b=17.225(3)$ Å	$T=23$ °C
$c=12.380(2)$ Å	$\lambda=0.7106$ Å
	$\rho_{calc}=2.07$ g cm^{-3}
$\beta=99.29(2)$°	$\mu=100.8$ cm^{-1}
$V=1786.1$ Å^3	Transmission coeffcient=0.33–0.94
$Z=4$	$R(F_0)=0.0841$ (=0.1329, all reflection)
	$R_w(F_0)=0.0711$ (=0.0784, all reflection)

II. EXPERIMENTAL

A. Synthesis and crystal structure

The crystals were prepared by slow evaporation of a solution of piperidinium bromide [(pipdH)Br] (0.02 mol, 3.32 g) and $CuBr_2$ (0.04 mol, 8.93 g) in 225 ml of ethanol. After about 2 weeks, small shiny black crystals of $(pipdH)_2CuBr_4$ were formed. Slow evaporation of a solution of the same stoichiometric ratios of (pipdH)Br and $CuBr_2$ in methanol produced $(pipdH)CuBr_3$ crystals.

The data collection for the crystal-structure determination was carried out using a Syntex $P2_1$ diffractometer upgraded to Nicolet $R3m$ specifications. A Mo $K\alpha$ radiation source ($\lambda=0.71069$ Å) with a graphite monochromator was used.[12] The orientation matrix and lattice parameters were optimized from a least-squares calculation on 25 carefull centered reflections in the range $21°<2\theta<26°$. Two standard reflections (013, 040) were monitored every 96 reflections and showed no systematic variation. The intensities of 2585 reflections were measured using an ω scan (1.0° range) with speeds varying from 4°–29.3°/min. Following the data reduction, 2309 unique reflections remained, with 1428 having $|F|>3\sigma$. The positions of all atoms were estimated from those of the isostructural $(pipdH)_2CuCl_4$ compound.[13] All nonhydrogen atoms were refined anisotropically to a final $R=0.0841$ and $R_w=0.0711$. The final refinement included 155 least-squares parameters. The goodness of fit was 1.444 and the final difference map showed a residual of $2e^-$/Å^3 near Br(1). This rather large residual could not be included in the final refinement in a meaningful way, i.e., it did not correspond to a disordered Br(1) site. The hydrogen atoms were refined isotropically with the C-H and N-H distances fixed at 0.96 Å and the isotropic thermal parameters fixed at 1.2 times the equivalent isotropic U of the atom to which they were bonded. An absorption coefficient was calculated to be 100.8 cm^{-1} and empirical absorption corrections were applied (transmission range is 0.33–0.94). All data reduction, including Lorentz and polarization corrections, structure solution and refinement, and graphics were performed using SHELXTL 5.1 software.[14] Table I gives a summary of important crystal and refinement parameters. Positional coordinates are given in Table II, interatomic distances and angles in Table III, and nonbonded distances and angles in Table IV.

TABLE II. Atomic coordinates ($\times 10^4$) and isotropic thermal parameters for bis(piperidinium)tetrabromocuprte(II).

	x	y	z	U^a
Cu	6952(3)	799(2)	2421(2)	44(1)
Br(1)	7071(3)	−418(1)	1538(2)	53(1)
Br(2)	9391(3)	1324(1)	2011(2)	55(1)
Br(3)	4330(3)	1173(2)	1609(2)	56(1)
Br(4)	6907(3)	1210(1)	4223(2)	53(1)
N(1)	2937(22)	−737(10)	682(12)	49(8)
C(2)	1530(29)	−511(14)	1146(18)	62(11)
C(3)	1830(31)	−665(15)	2401(21)	75(13)
C(4)	2201(33)	−1508(16)	2570(18)	76(13)
C(5)	3594(31)	−1752(15)	2059(17)	73(12)
C(6)	3321(31)	−1563(13)	882(16)	61(11)
N(11)	2753(23)	1436(10)	3926(13)	60(8)
C(12)	2751(30)	2275(12)	4292(17)	67(11)
C(13)	1391(27)	2426(12)	4819(17)	62(11)
C(14)	1381(34)	1897(17)	5769(19)	93(15)
C(15)	1446(29)	1069(16)	5471(21)	78(12)
C(16)	2798(26)	904(12)	4896(18)	58(10)

[a]The equivalent isotropic U is defined as one-third of the trace of the orthogonalized U_{ij} tensor.

B. Magnetic-susceptibility measurements

The temperature-dependent powder-sample magnetic-susceptibility data were collected at Montana State Uni-

TABLE III. Selected bond distances and angles for bis(piperidinium)tetrabromocuprate(II).

Bond distances (Å)	
Cu—Br(1)	2.373(4)
Cu—Br(2)	2.388(4)
Cu—Br(3)	2.378(3)
Cu—Br(4)	2.347(3)
Bond angles (deg)	
Br(1)—Cu—Br(2)	97.7(1)
Br(1)—Cu—Br(3)	98.7(1)
Br(2)—Cu—Br(3)	126.3(1)
Br(1)—Cu—Br(4)	135.5(1)
Br(2)—Cu—Br(4)	103.6(1)
Br(3)—Cu—Br(4)	99.3(1)

TABLE IV. Nonbonded distances and angles for bis(piperidinium)tetrabromocuprate(II). All nonbonded distances greater than 6 Å were omitted. (a) denotes bromides related by a center of inversion; (b) denotes bromides related by a translation.

Atoms	Distances (Å)	Atoms	Angles (deg)
Br(1)-Br(1a)	4.961	Cu-Br(3)-Br(2b)	146.0
Br(1)-Br(3a)	4.098	Br(3)-Br(2b)-Cu(b)	153.5
Br(2)-Br(3b)	4.308	Cu-Br(1)-Br(3a)	133.7
		Br(1)-Br(3a)-Cu(a)	115.1
		Cu-Br(1)-Br(1a)	91.1
Br(1)-C(2)	4.652	Br(1)-N(1)-C(2)	132.5
Br(1)-C(3)	4.758	Br(1)-N(1)-C(6)	85.3
Br(1)-C(4)	4.892	Br(1)-N(11)-C(12)	133.4
Br(1)-C(5)	3.875	Br(1)-N(1)-C(6)	140.7
Br(1)-C(6)	3.720	Br(1)-N(11)-C(16)	97.5
Br(1)-N(1)	3.540		
Br(1)-N(11)	5.989		
Br(3)-C(6)	4.847	Br(3)-N(1)-C(2)	83.1
Br(3)-N(1)	3.618	Br(3)-N(11)-C(12)	113.7
Br(3)-C(2)	3.734	Br(3)-N(11)-C(16)	129.1
Br(3)-N(11)	3.386		
Br(3)-C(12)	4.228		
Br(3)-C(16)	4.491		
Br(4)-N(11)	3.507	Br(4)-N(11)-C(12)	97.1
Br(4)-C(12)	3.989	Br(4)-N(11)-C(16)	87.3
Br(4)-C(16)	3.752		

versity on a Princeton Applied Research 155 vibrating-sample magnetometer. Measurements were made in the temperature range 5.6 to 123.8 K. The field was 5000 G throughtout the entire data collection, and a separate field versus magnetization data collection from 0 to 5000 G showed no saturation.

C. EPR data collection

Data were collected at room temperature using the E-3 Varian *X*-band EPR spectrometer. The crystal axes were identified using an x-ray precession camera. The crystal was mounted on a Kel-F sleeve attached to one end of a quartz rod which passed through a goniometer head. EPR spectra were taken by successively rotating the crystal about three mutually perpendicular axes (a,b,c^*). In the b-c^* plane, the digitized spectra were recorded using an Apple IIe computer. These digitized data were transferred to the Washington State University mainframe computer for further analysis.

III. RESULTS

A. Structure description

At first glance this compound appears to consist of discrete, distorted $CuBr_4^{2-}$ tetrahedra, co-crystallized with the piperidinium cations. The tetrahedra are flattened, showing *trans* angles of 126.3° and 135.3°, with the other angles ranging from 97.7° to 103.6°. The Cu—Br bond distances range from 2.347 to 2.388 Å. If the Br · · · Br contacts between monomers are considered, chains of weakly interacting dimeric units become apparent (Fig. 1). As can be seen in Fig. 1, the Br · · · Br contacts linking the monomers into magnetic dimer units are 4.10 Å, while the contacts between dimers are 4.31 Å. The two $CuBr_4^{2-}$ monomers composing each dimer are related by a center of inversion, thus making the copper(II) ions in each dimer crystallographically and magnetically equivalent. These dimer pairs are joined together to form a double chain running along the a axis,

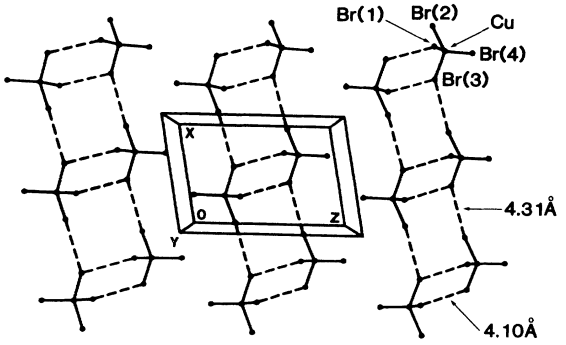

FIG. 1. Packing arrangement of the $CuBr_4^{2-}$ monomers as viewed down the b axis.

each dimer along the chain related by a unit-cell translation. These chains of dimers are related to a set of crystallographically equivalent chains (not shown in Fig. 1) by a c glide operation. The cations form a network of bridging hydrogen bonds between the $CuBr_4^{2-}$ tetrahedra. The structure is isomorphous to the corresponding chloride salt.[13]

B. Magnetic-susceptibility data

A plot of the magnetic susceptibility versus temperature data is shown in Fig. 2. The squares represent the individual data points, while the solid line shows the theoretical fit as described below. The sharp peak observed in the curve appears at approximately 8 K.

The double-chain structure leads to a ladder-type magnetic system with an intradimer exchange, J, defining the rungs and an interdimer coupling, J', defining the rails. Since no model exists to describe the magnetism of this type of system, an alternating-chain model[15] was used to fit the data. Assuming isotropic exchange coupling, the Hamiltonian for such a system may be written as

$$\mathcal{H}=-2J\sum_{i=1}^{n/2}(\mathbf{S}_{2i}\cdot\mathbf{S}_{2i-1}+\alpha\mathbf{S}_{2i}\cdot\mathbf{S}_{2i+1}) , \quad (1)$$

where J is the intradimer exchange interaction and α is the alternation parameter.[15] The interdimer exchange interaction is given by $J'=\frac{1}{2}\alpha J$. The expression derived for the susceptibility is

$$\chi_m=\frac{Ng^2\mu_B^2}{kT}\frac{A+Bx+Cx^2}{1+Dx+Ex^2+Fx^3} , \quad (2)$$

where $x=|J|/kT$, and the coefficients $A-F$, all functions of α, are found in the above-referenced paper by Hatfield and co-workers.[15] A nonlinear least-squares fit, varying α, J, and g, was used to fit this expression to the data. This fit yielded $J/k=-6.64(2)$ K, $\alpha=0.20(2)$, and $g=2.210(6)$. This corresponds to an intradimer exchange of $J/k=-6.64$ K and an interdimer exchange of $J'/k=\alpha J/k=-0.66$ K. This g value is somewhat larger than the value of 2.13 for g_{ave} obtained from the EPR study. However, this discrepancy is not surprising considering the inadequacy of the magnetic model to account for all of the actual exchange pathways.

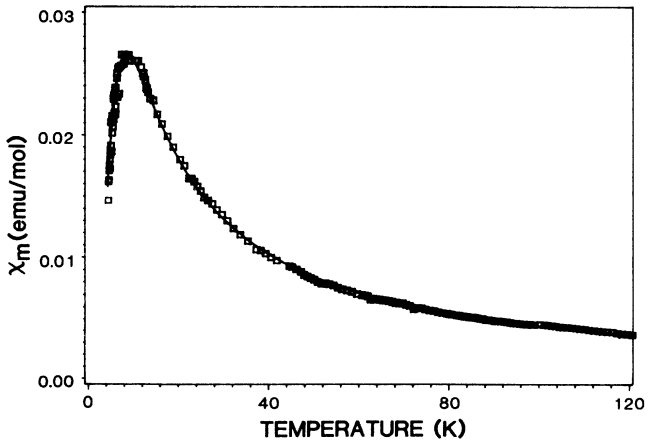

FIG. 2. The magnetic susceptibility as a function of temperature. The solid curve represents the best fit to the alternating chain model.

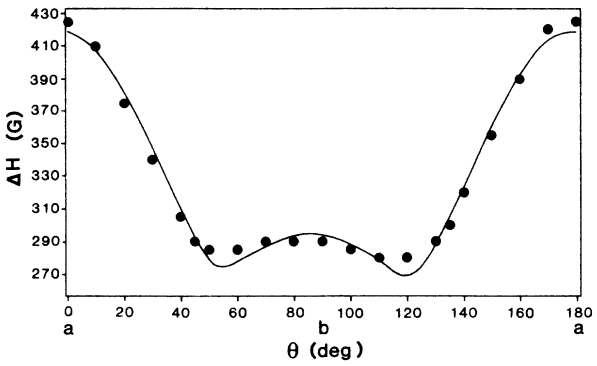

FIG. 3. Angular variation at room temperature of the linewidth in a-b plane. Solid curve is the best fit of the experimental data to Eq. (3), with parameters $A=256.7$ G, $B=60.3$ G, $C=42.6$ G, and $\theta_1=0°$, and $\theta_2=-2.6°$. A minimum in linewidth between $\theta=0°$ and $\theta=90°$ is indicative of spin-diffusion relaxation processes.

C. EPR results

In the a-b and a-c^* planes, the EPR spectra consisted of a single line at all orientations. The results of linewidth measurements in the a-b and a-c^* planes are plotted in Figs. 3 and 4, respectively. In both planes, the linewidths have minima at angles intermediate between the crystal axes. This is typical of behavior associated with long-time spin-diffusion effects. Based on the structural characteristics, this is assumed to be one dimensional in nature. The presence of small (1–10%) amounts of spin anisotropy in the exchange interaction is typical in copper halide systems and leads to short-time relaxation processes. These give rise to an angular depen-

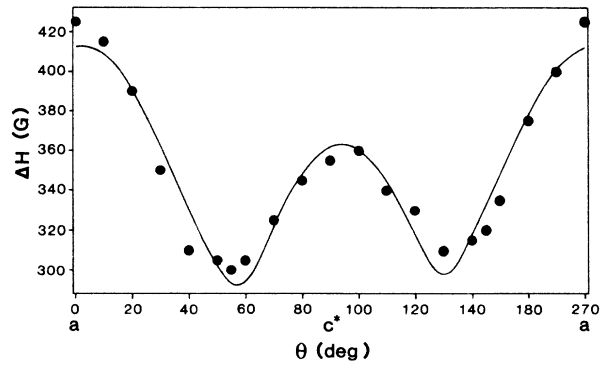

FIG. 4. Angular variation of the linewidth at room temperature in the a-c^* plane. Solid curve is the best fit of the experimental data to Eq. (3), with parameters $A=306.3$ G, $B=-38.2$ G, $C=57.3$ G, $\theta_1=8.7°$ and $\theta_2=3.3°$. A minimum in linewidth between $\theta=0$ and $\theta=90°$ is again indicative of the presence of spin-diffusion relaxation processes.

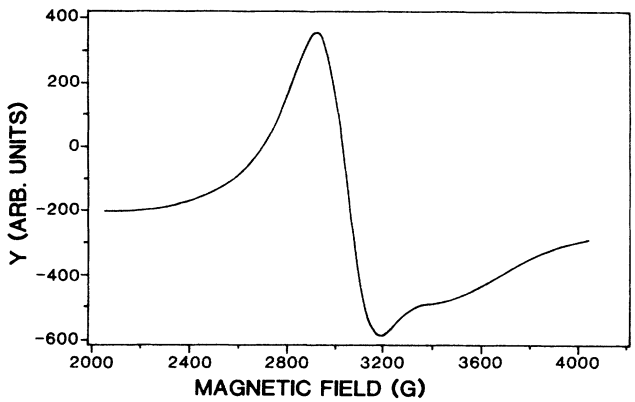

FIG. 5. A typical EPR spectrum in the b-c^* plane. Actual spectrum and the data fitted to Eq. (5) coincide. Parameters evaluated are $H_\alpha=3042$ G, $H_\beta=3338$ G, $\Delta H_\alpha=234$ G, $\Delta H_\beta=444$ G, and $J_i/k=0.002$ K.

dence to the EPR linewidths similar to that for dipolar interactions.[16] The solid line in each figure represents the best fit of the experimental data to the theoretical model given by

$$\Delta H = A + B\cos^2(\theta-\theta_1)+C|3\cos^2(\theta-\theta_2)-1|^{4/3}\ , \quad (3)$$

where A and B terms arise from contributions from spin anisotropies and the last term arises from long-time spin-diffusive processes, while θ is the angle between the applied magnetic field and the a crystallographic axis. The separate angular parameters θ_1 and θ_2 are included not only to account for possible crystal misorientation, but also to emphasize that the spin-diffusion axis and the spin-anisotropy axis do not have to coincide. The parameters calculated from a nonlinear least-squares fit of the experimental data to (3) are given in Figs. 3 and 4. We thus see that there appears to be significant contributions to linewidth from both spin anisotropies and spin diffusion, and that their principal axes are nearly parallel in these two planes. In particular, the θ_2 values indicate the spin-diffusion axis is parallel to the a axis within experimental error.

The g-factor data in the a-b and a-c^* planes showed the usual sinusoidal angular behavior. The experimental data were accurately reproduced by the general expression

$$g = g_0 + g_1\cos^2(\theta-\theta_0) \quad (4)$$

with $g_0=2.179$, $g_1=-0.119$, $\theta_0=-2.2°$ for the data in the a-c^* plane and $g_0=2.157$, $g_1=-0.096$, $\theta_0=-2.7°$ in the a-b plane. Again, θ is the angle between the applied magnetic field and the a axis and θ_0 takes into account the possible orientational error between the crystallographic and g-factor axes. As can be seen from the data fit, the crystallographic axes and the g-factor axes are nearly parallel in these planes.

In the b-c^* plane, the EPR spectrum at various orientations of the magnetic field is superposition of spectra from two magnetically inequivalent sites. A typical spectrum in this plane is shown in Fig. 5. Linewidths corresponding to each site and the interaction between the sites were calculated by a nonlinear least-squares fit of the digitized spectrum at each orientation to the theoretical model developed by Hoffman,[17]

$$Y(H)=N\frac{[W_2-2(H-H_0)J_i](W_1^2+W_2^2)-4[(H-H_0)W_2-(\Gamma_0+2J_i)W_1][H-H_0)W_1+(\Gamma_0+J_i)W_2]}{(W_1^2+W_2^2)^2} \quad (5)$$

where

$$W_1=(H-H_\alpha)(H-H_\beta)-(\Gamma_\alpha+J_i)(\Gamma_\beta+J_i)+J_i^2\ ,$$

$$W_2=(H-H_\beta)(\Gamma_\beta+J_i)+(H-H_\beta)(\Gamma_\alpha+J_i)\ .$$

H_α and H_β are the resonance fields corresponding to magnetically inequivalent sites α and β, respectively, and Γ_α and Γ_β are the corresponding linewidths. J_i is the magnitude of the exchange interaction between the magnetically inequivalent sites α and β. The quantities H_0 and Γ_0 in (5) are the average resonance field and average linewidth, defined as $H_0=(H_\alpha+H_\beta)/2$ and $\Gamma_0=(\Gamma_\alpha+\Gamma_\beta)/2$. The peak-to-peak linewidth, ΔH, of the derivative spectrum is related to Γ as $\Gamma=(\sqrt{3}/2)\Delta H$. N in (5) is a normalization constant. All quantities in (5) are expressed in gauss. Figure 5 is actually, a superposition of the actual spectrum and the fit of the digitized spectrum to (5). The fit is, to all intents, exact.

The results of the measurements in the b-c^* plane are plotted in Figs. 6 and 7 for the linewidth, ΔH, and the g factor, respectively. The linewidths show a simple $\cos^2$ angular dependence, indicating the presence of spin-anisotropy effects only. Since this plane is perpendicular to the a axis ($\theta=90°$), contribution from spin diffusion will be constant. Thus, in Fig. 6 the solid lines are the best fit of the linewidth data to the equation

$$\Delta H = A + B\cos^2(\phi-\phi_1)\ , \quad (6)$$

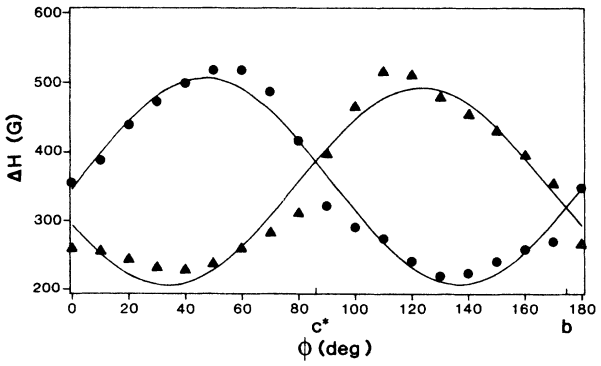

FIG. 6. Angular variation of the linewidth at room temperature in the b-c^* plane; data for site α (●), data for site β (▲). Solid curves are the best fit of the data to Eq. (6). All data were generated by a nonlinear least-squares fit of the digitized spectrum at each orientation to Eq. (5).

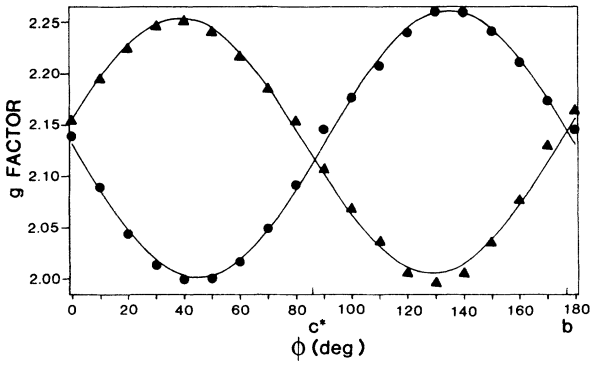

FIG. 7. Angular variation of the g factor in the b-c^* plane; data for site α (●), data for site β (▲). Solid curves are the best fit of the data to Eq. (4) with θ replaced by ϕ and θ_0 by ϕ_0. All data were generated by a nonlinear least-squares fit of the digitized spectrum at each orientation to Eq. (5).

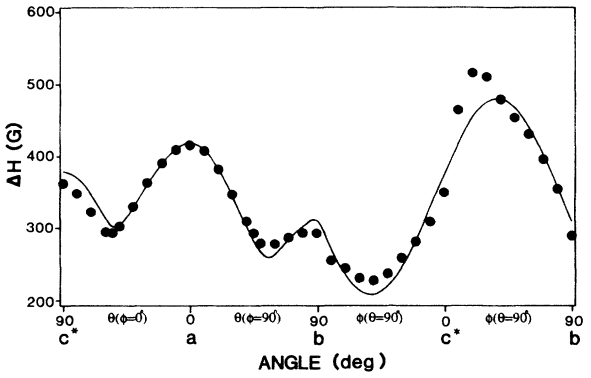

FIG. 8. A composite plot of the angular variation of the linewidth at room temperature. Solid curve represents the best fit of the data to Eq. (7), with parameters $A=420.5$ G, $B_1=-154.6$ G, $B_2=-272.6$ G, $C=60.8$ G, and $\phi_1=57°$.

where ϕ is the angle between the applied magnetic field and the b axis. The parameter ϕ_1 takes into account the possible misorientation between the crystallographic and the magnetic axes. The various parameters calculated are $A_\alpha=492$ G, $B_\alpha=-286$ G, $\phi_{1\alpha}=35.5°$ for the site α and $A_\beta=507$ G, $B_\beta=-298$ G, $\phi_{1\beta}=-46.8°$ for the site β. The solid lines in Fig. 7 are the best fit of the g-factor data to (4) with θ replaced by ϕ and θ_0 by ϕ_0. The various parameters are $g_{0\alpha}=2.294$, $g_{1\alpha}=-0.248$, $\phi_{0\alpha}=-51.4°$ for the site α and $g_{0\beta}=2.301$, $g_{1\beta}=-0.260$, $\phi_{0\beta}=42.8°$ for the site β. For both the ΔH- and g-value data, some small experimental variations exist between the two equivalent sites due to misorientation of the rotation axes of the crystal. Nevertheless, the data are essentially equivalent. From this analysis, it can be seen that in this plane the crystallographic axes are not coincident with the principal axes of either the local anisotropy or the g tensor. However, the g-tensor and local-anisotropy axes are essentially coincident.

The linewidth data in all the planes are adequately reproduced by contributions from spin anisotropies and spin-diffusion effects as represented by the general expression[18,19]

$$\Delta H(\theta,\phi)=A+B_1\cos^2\theta+B_2\sin^2\theta\cos^2(\phi-\phi_1)+C(3\cos^2\theta-1)^{4/3}, \quad (7)$$

where θ and ϕ are the polar and azimuthal angles of the magnetic field. Angle θ is measured from the a crystallographic axis, whereas ϕ is measured from the b axis. The angular parameter ϕ_1 is included to take into account the mismatch of the crystallographic and the magnetic axes in the b-c^* plane as seen earlier in the context of (5) and (6). The data for the α site and the best fit are shown in Fig. 8. The various parameters calculated are $A=420$ G, $B_1=-155$ G, $B_2=-273$ G, $C=61$ G, and $\phi_1=57°$. The g-factor data in all the planes are fitted to the general expression

$$g(\theta,\phi)=g_0+g_1\cos^2\theta+g_2\sin^2\theta\cos^2(\phi-\phi_0). \quad (8)$$

The data and the best fit are shown in Fig. 9. The various parameters are $g_0=2.045$, $g_1=0.018$, $g_2=0.245$, and $\phi_0=40.3°$. These g-value parameters are essentially identical with those obtained from fitting the individual planes separately. For the ΔH parameters, some differences with the values from the individual planes are found. In particular, the contribution arising from the spin-diffusion term is enhanced.

The direction cosines for the pseudo-S_4 axis of the $CuBr_4^{2-}$ tetrahedra are calculated from the x-ray data to be 87.0°, 41.8°, and 49.4°. The direction cosines of $g_\parallel$ determined from the diagonalization of the g-factor for the β site were found to be 90.0°, 40.3°, and 49.7°. Thus $g_\parallel$ coincides with the psuedo-S_4 axis of the local $CuBr_4^{2-}$ tetrahedra within the experimental error. The values of the diagonalized g factor are 2.290, 2.063, and 2.045. The direction cosines for $\Delta H_\parallel$ were found to be 97.9°, 36.3°, and 54.9°. There is, thus, some small amount of misalignment ($<10°$) between the $\Delta H_\parallel$ axis and the local S_4 axis.

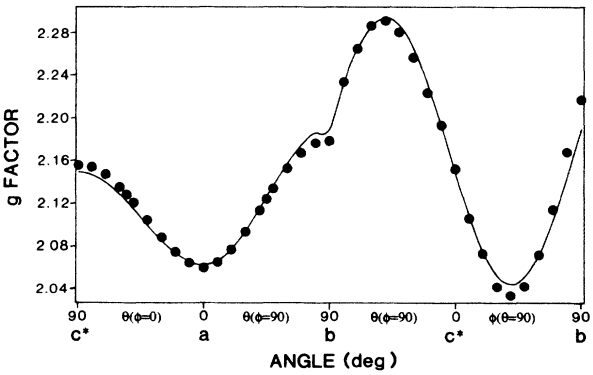

FIG. 9. A composite plot of the angular variation of the g factor. Solid curve is the best fit of the data to Eq. (8). The parameters calculated are $g=2.022$, $g_1=0.052$, $g_2=0.244$, and $\phi_0=40.9°$.

IV. SUMMARY

The x-ray diffraction studies reveal that structurally the compound $(pipdH)_2CuBr_4$ is comprised of isolated monomeric $CuBr_4^{2-}$ units. Intermonomer contacts define a magnetic ladder system. From magnetic-susceptibility measurements, the magnetic system is characterized as exchange-coupled $CuBr_4^{2-}$ dimers with intradimer interaction, $J/k = -6.64$ K, with a weaker ($J'/k = -0.66$ K) coupling between these dimeric units. The room-temperature EPR data in the a-c^* and a-b planes indicate the presence of strong spin-diffusive relaxation processes, defining the system as a linear chain propagating along the a axis. In the b-c^* plane, the EPR spectra are the superposition of spectra corresponding to magnetically inequivalent sites in the unit cell. The interaction between these sites is determined to be equal to 0.002 K. The principal axes corresponding to $g_{\|}$ lies along the psuedo-S_4 axis of the local $CuBr_4^{2-}$ tetrahedra. The principal axes of the component of the linewidths ascribed to spin anisotropy effects are nearly coincident with those for the g tensor. Thus, the orientation of the components of the spin anisotropies mirror, in some fashion, the g-tensor anisotropy.

SUPPLEMENTARY MATERIAL

Tables of x-ray data-collection parameters, bond lengths and angles, anisotropic thermal parameters for nonhydrogen atoms, and hydrogen-atom positions and isotropic thermal parameters (four pages), and structure-factor tables (14 pages) are available from the authors.

ACKNOWLEDGMENTS

Support of the National Science Foundation (NSF) through Grant No. DMR-88-0332 and the Boeing Company for the purchase of the x-ray diffraction system is gratefully acknowledged. Authors are thankful to Professor J. E. Drumheller of the Department of Physics, Montant State University, (Bozeman, MT) for providing the facilities to do magnetic-susceptibility measurements.

---

*Present address: Baker Laboratory, Department of Chemistry, Cornell University, Ithaca, NY 14853-1301.

[1]J. C. Bonner, J. Magn. Magn. Mater. **15-18**, 1003 (1980).

[2]R. D. Willett, in *Magneto-Structural Correlations in Exchange Coupled Systems,* edited by R. D. Willett, D. Gatteschi, and O. Kahn (Reidel, Boston, 1985), p. 389.

[3]R. D. Willett and C. P. Landee, J. Appl. Phys. **52**, 2004 (1981).

[4]K. Kopinga, A. M. C. Tinus, W. J. M. de Jonge, and G. C. de Vries, Phys. Rev. B **36**, 5398 (1987).

[5]R. D. Willett, R. J. Wong, and M. Numata, Inorg. Chem. **22**, 3189 (1983); R. D. Willett, H. Place, and M. Middleton, J. Am. Chem. Soc. **110**, 8639 (1988).

[6]T. E. Grigereit and R. D. Willett, J. Appl. Phys. **61**, 3292 (1987).

[7]C. P. Landee, A. Djili, D. F. Mudgett, M. Newhall, H. Place, B. Scott, and R. D. Willett, Inorg. Chem. **27**, 620 (1988).

[8]G. V. Rubenacker, D. N. Haines, J. E. Drumheller, and K. Emerson, J. Magn. Magn. Mater. **43**, 238 (1984).

[9]J. T. Blanchette and R. D. Willett, Inorg. Chem. **27**, 843 (1988).

[10]L. J. de Jonge and A. L. Miedema, Adv. Phys. **23**, 1 (1974).

[11]J. E. Drumheller, Magn. Reson. Rev. **7**, 123 (1982).

[12]C. F. Campana, D. F. Shepard, and W. M. Litchman, Inorg. Chem. **20**, 4039 (1981).

[13]V. Fernandez, M. Moran, M. T. Gutierez-Rios, C. Foces-Foces, and F. H. Cano, Inorg. Chem. Acta. **128**, 239 (1987).

[14]G. Sheldrick, SHELXTL, Nicolet Analytical Instruments, Madison, Wi (1984).

[15]J. W. Hall, W. E. Marsh, R. R. Weller, W. E. Hatfield, Inorg. Chem. **20**, 1033 (1981).

[16]Z. G. Soos, K. T. McGregor, T. I. P. Cheng, and A. J. Silverstein, Phys. Rev. B **16**, 3036 (1977).

[17]S. K. Hoffmann, Chem. Phys. Lett. **98**, 329 (1983).

[18]P. M. Richards, in *Low-Dimensional Cooperative Phenomena,* edited by H. J. Keller (Plenum, New York, 1974), p. 171.

[19]R. D. Willett, R. Wong, and M. Numata, J. Magn. Magn. Mater. **15–18**, 717 (1980).